Biochemical and Biophysical Research Communications 446 (2014) 945–951

Contents lists available at ScienceDirect

Biochemical and Biophysical Research Communications

journal homepage: www.elsevier.com/locate/ybbrc

Crystal structure of the single-stranded RNA binding protein HutP from *Geobacillus thermodenitrificans*

Viswanathan Thiruselvam [a], Padavattan Sivaraman [b], Thirumananseri Kumarevel [b,c,*], Mondikalipudur Nanjappagounder Ponnuswamy [a,*]

[a] Centre of Advanced Study in Crystallography and Biophysics, University of Madras, Guindy Campus, Chennai 600 025, India
[b] RIKEN SPring-8 Center, Harima Institute, 1-1-1 Kuoto, Sayo, Hyogo 679-5148, Japan
[c] Structural Biology Laboratory, RIKEN Yokohama Institute, RIKEN, 1-7-22 Suehiro-cho, Tsurumi, Yokohama 230-0045, Japan

ARTICLE INFO

Article history:
Received 27 February 2014
Available online 17 March 2014

Keywords:
RNA binding
Antitermination
HutP
Gene regulation
Geobacillus thermodenitrificans

ABSTRACT

RNA binding proteins control gene expression by the attenuation/antitermination mechanism. HutP is an RNA binding antitermination protein. It regulates the expression of *hut* operon when it binds with RNA by modulating the secondary structure of single-stranded *hut* mRNA. HutP necessitates the presence of L-histidine and divalent metal ion to bind with RNA. Herein, we report the crystal structures of ternary complex (HutP–L-histidine–Mg^{2+}) and EDTA (0.5 M) treated ternary complex (HutP–L-histidine–Mg^{2+}), solved at 1.9 Å and 2.5 Å resolutions, respectively, from *Geobacillus thermodenitrificans*. The addition of 0.5 M EDTA does not affect the overall metal-ion mediated ternary complex structure and however, the metal ions at the non-specific binding sites are chelated, as evidenced from the results of structural features.

1. Introduction

Expression of bacterial operons is controlled at the transcriptional level. RNA binding proteins regulate this kind of mechanism, which either act as activator/repressor or by modulating the structure of the corresponding RNA. The site responsible for the transcription mechanism of operon is located within or at the end of the operons [1]. Gene expression through transcription regulation in operons is referred as transcriptional attenuation and antitermination [2]. Protein mediated antitermination mechanism is described in nine operons, out of which eight from the catabolic system. Basically six operons are found in *Bacillus subtillis* [3].

Antitermination proteins from *B. subtilis* are classified as (i) bgl-Sac family (ii) glP and (iii) *hutP* types of operons based on the mode of regulation. Antitermination/attenuation mechanism of gene regulation in many systems, such as TRAP, hutP, pgR, bglP, sacT, glpP, licT, SacY, amir and nasR are reported earlier [3]. The antitermination that leads to full-length transcription of genes by (i) modification in RNA polymerase and (ii) destabilizing the terminator structure. The TRAP attenuation process is carried out in *trp* operon. In the presence of tryptophan, 11 subunits of TRAP bind with trp leader mRNA and induce the terminator [4] whereas in the absence of tryptophan, TRAP is unable to bind with mRNA due to the formation of an alternative conformation. This kind of regulation is named as negative regulation [5–7].

In hutP, histidine is an important and essential amino acid, synthesized in cells involving different steps of biochemical mechanism. When nitrogen and carbohydrates are lacking in their sources, its *hut* operon gets activated and utilize the freely available histidines as nitrogen source. The *hutP* gene is located near the promoter in *hut* operon with five additional genes *hutH*, *hutU*, *hutI*, *hutG* and *hutM*, which are located downstream from *hutP* and the promoter [8–11].

Hexameric form of HutP binds with specific sequence of *hut* mRNA in the presence of L-histidine [10]. HutP not only requires L-histidine for RNA binding but also requires divalent metal ions like Mg^{2+}, Mn^{2+} [12]. In the apo-form, HutP crystallized as a dimer and three dimers were related by 3-fold symmetry to form the hexamer. In binary complex, HutP recognizes the L-histidine at the dimer interface by forming an open hydrophobic pocket with its surrounding residues. This hydrophobic pocket is essential to clarify whether the incoming residues possesses the imidazole group or not. HutP–L-histidine binding with mRNA confirms that the L-histidine analogs with imidazole ring possess higher affinity

* Corresponding authors. Address: Structural Biology Laboratory, RIKEN Yokohama Institute, RIKEN, 1-7-22 Suehiro-cho, Tsurumi, Yokohama 230-0045, Japan. Fax: +81 45 503 9480 (T. Kumarevel). Fax: +91 44 2230 0122 (M.N. Ponnuswamy).

E-mail addresses: Kumarevel.thirumananseri@riken.jp (T. Kumarevel), mnpsy@hotmail.com (M.N. Ponnuswamy).

http://dx.doi.org/10.1016/j.bbrc.2014.03.036
0006-291X/

for binding [13]. Once the ternary complex (HutP–L-histidine–Mg^{2+}) was achieved, the metal ion makes the structural rearrangement in L3 and L5 loop regions and L-histidine binding sites in the structure. These structural rearrangements are responsible for recognition of RNA. Upon binding to the HutP, RNA terminator structure is destabilized and changed its conformation in a novel triangular fashion; but the protein will not go for any further conformational changes. Thus, divalent metal ions play crucial role in HutP–RNA interactions and structural rearrangement of HutP–RNA complex formation [14].

The literature survey reveals that *hutP* gene also exists in other *Bacillus* species including *Bacillus anthracis, Bacillus cereus* [15], *Bacillus halodurans* [16], *Geobacillus kautophilus* [17] and *Bacillus amyloliquefaciens* [18].

Recent study indicates the availability of *hutP* gene in *Geobacillus hermodenitrificans* that it is a facultative aerobic thermophilic bacterium. It was isolated from oilfield in Dagang (Northern China) at a depth of 2000 m and a temperature of 73 °C. The complete genome sequence consists of 3,550,319-bp chromosome and 57,693-bp plasmid and the *hutP* gene consists of 149 amino acids [19]. About 60% sequence similarity is observed between *G. thermodenitrificans* and *B. subtilis*. Thermophilic proteins differ from mesophilic in structure and function and remain stable around 73 °C. In view of the above reasons, we plan to determine the crystal structures of HutP–L-histidine–Mg^{2+} and HutP–L-histidine–Mg^{2+}–RNA to understand the RNA binding mechanism of HutP from *G. thermodenitrificans.*

In this present study, we show the ternary complex structure (HutP–L-histidine–Mg^{2+}) of antitermination protein HutP. The importance of L-histidine and Mg^{2+} ions for RNA binding is also demonstrated by biochemical studies. To understand the role of metal ion, we solved the EDTA treated ternary complex structure.

2. Materials and methods

2.1. Cloning, expression and purification

The *hutP* gene from *G. thermodenitrificans* was chemically synthesized with His-tag and cloned into PCR 2.1vector. The cloned gene was sub-cloned by digesting with *Nde*I and *BamH*I enzymes, and the resultant fragment was inserted into pHCE constitutive expression vector containing a His6-tag and thrombin cleavage site at the N-terminus, which was digested earlier with the same enzyme. The positive clones was confirmed by DNA sequencing and transformed into BL21(DE3) cells. The recombinant strain was expressed overnight in LB medium containing 50 μg/ml ampicillin without any inducer such as IPTG [20]. Cells were harvested by centrifugation at 8000 rpm for 15 min and the pellet was resuspended in a 50 ml of purification buffer containing 50 mM Tris–HCl, 500 mM NaCl, 5% glycerol and 2 mM β-mercaptoethanol. The cells were lysed by sonication for 10 min with 1 min interval in ice-cold condition. Protein containing the supernatant was separated from lysate through centrifugation for about 15,000 rpm for 10 min.

The his-tagged protein was purified using Ni–NTA column. The column is pre equilibrated with buffer containing 50 mM Tris–HCl, 500 mM NaCl, 5% glycerol and 2 mM β-mercaptoethanol. The protein sample was applied to the column and elution was carried out by imidazole gradient method. HutP protein eluted at 300 mM of imidazole gradient and was confirmed by SDS–PAGE. The imidazole has been removed from protein through dialysis with the same equilibration buffer.

Later, the engineered his-tag was removed by thrombin digestion. The his-tag containing protein sample digested by adding thrombin (1.5 U/mg) for 2 h, digestion was confirmed by SDS–PAGE. The digested sample was applied into HiTtrap QFF column and the bound sample was eluted by salt gradient method. The purity of protein was confirmed in SDS–PAGE (Fig. 1A).

2.2. Crystallization

Purified protein sample was concentrated (14 mg/ml) and used for crystallization. Initial screening of HutP crystallization was performed by hanging drop vapour-diffusion method using the following kits, Wizard screen I & II (Emerald Bio Systems), Hampton crystallization kits crystal screen and crystal screen 2 and MPD suite I & II. All the crystallization experiments were performed at 293 K. For HutP–L-histidine–Mg^{2+} complex, we have mixed 1 μL of protein solution, 1 μL each of 50 mM L-histidine and 10 mM $MgCl_2$, alongwith 3 μL of reservoir solution (1:1) and equilibrated against 500 μL reservoir solution. The preliminary crystals were appeared in Wizard I condition No. 26. The good quality single crystals suitable for diffraction were obtained within 3 days with the following condition; 10% W/V PEG 300; 0.1 M CHES pH 9.5 (Fig. 1B).

2.3. Data collection and processing

The crystals were cryo-protected with the mother liquor solution containing 15% glycerol and incubated for 3 min before data collection. Complete data set was collected at 1.9 Å resolution. For the EDTA-treated data, the crystal was soaked in the previous cryo condition (mother liquor plus15% glycerol) along with 0.5 M EDTA for about 1 min and the data set was collected up to 2.5 Å at 100 K using structural genomics beam line I, BL26B1, (SPring-8, Hyogo, Japan).

The soaking of the crystal in 0.5 M EDTA for longer time, for example, 1.5 and 2 min was also carried out, but unfortunately the crystal degradation had occurred and could not able to mount the crystal for data collection. Plausibly, crystal damage was caused by the chelation of metal ions.

The HutP protein crystal belonged to $P6_3$ space group with unit cell parameters $a = 90.811$; $b = 90.811$; $c = 76.672$. The Matthews co-efficient indicates the presence of two monomers in asymmetric unit with 56.98% solvent contents. The diffraction data sets were processed, integrated and scaled with HKL2000 (Table 1).

2.4. Gel mobility shift assay

The gel mobility shift assay was performed to clarify RNA binding with HutP protein. 21-mer RNA was purchased (Fasmac, Japan) and used for protein–RNA complex preparation. To analyze and understand the importance of L-histidine and $MgCl_2$, different complexes were prepared with varying concentrations as follows; HutP–RNA, HutP–RNA–L-histidine, HutP–RNA–$MgCl_2$ and HutP–RNA–L-histidine–$MgCl_2$. The shift of the band in gel was visualized using native gel electrophoresis. The conditions were optimized using different running buffer, binding buffer, pH, protein concentration, RNA, L-histidine and $MgCl_2$.

The prepared complexes were incubated in binding buffer containing 10 mM HEPES for about 15 min. Initially pre-run was allowed for 10 min/200 V at 4 °C and then the incubated sample was centrifuged and loaded after mixing with the dye. Protein–RNA complex was resolved through 6% non-denaturing polyacrylamide gel running 200 V at 4 °C. The gel was stained in SYBR green solution and visualized using Fuji film gel document instrument (Fig. 1C).

3. Results

3.1. Sequence and structure alignment

The protein sequence alignment was done using BLASTp [21]. A total of 93 hits observed in search against non-redundant database.

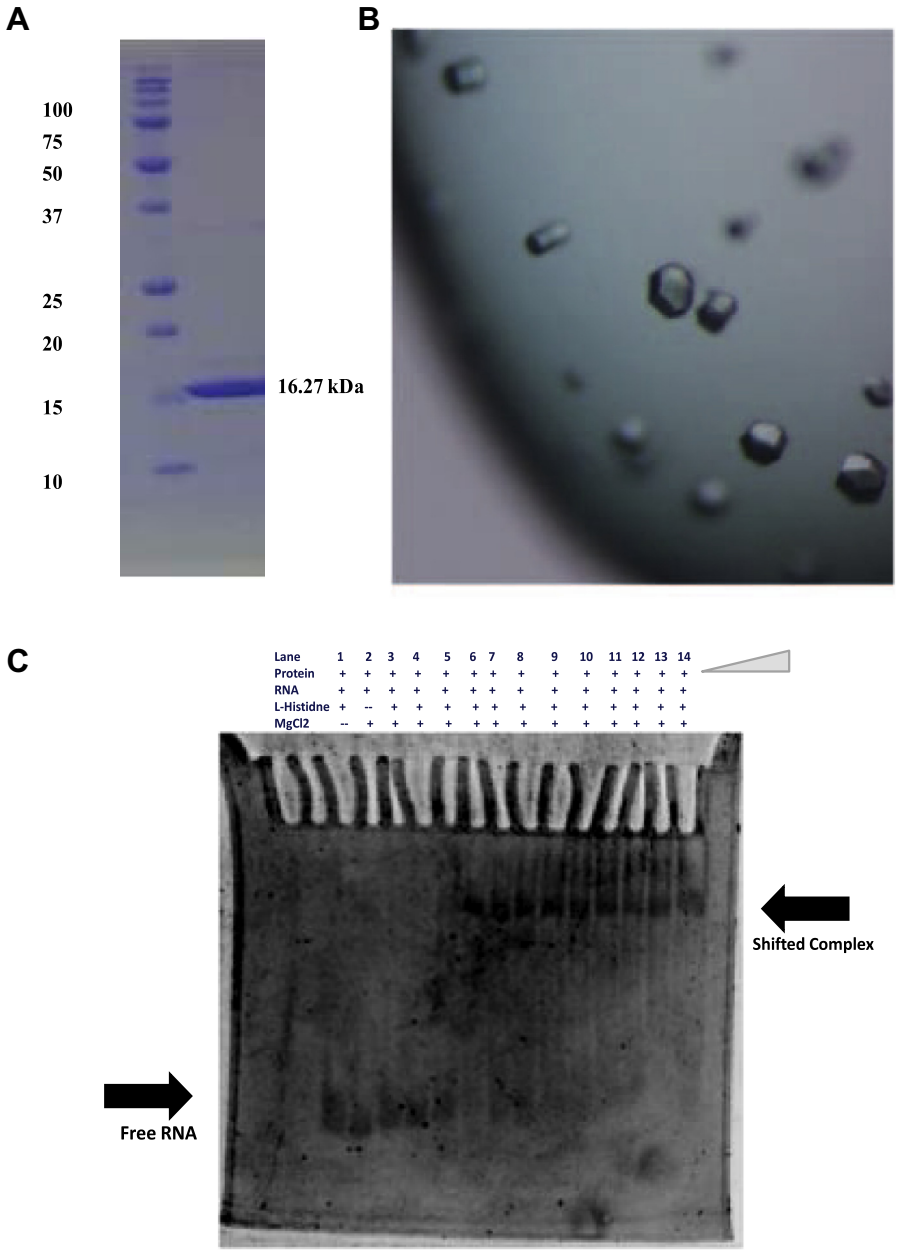

Fig. 1. HutP purification and RNA binding analysis. (A) SDS page results of purified HutP: Lane 1 standard markers; Lane 2 purified HutP 16 kDa (B) representative crystals of HutP-ternary complex (C) Gel-mobility shift assays showing the HutP–RNA complex formation. The arrow indicates the free RNA and shifted complex in the gel.

The sequence similarity of the related structures, which resemble from 87% to 19% species were taken for analysis. Interesting to note that the L-histidine binding residues 70Tyr, 82Glu, 89Arg, and 99Arg; Mg^{2+} binding residues 74His, 78His, and 139His; and the RNA binding residues 56Glu, 57Thr, 100Thr, 129Thr, and 138Glu are highly conserved and having 46–87% similarities, whereas the non-specific metal binding site residues are replaced in *G. thermodenitrificans*. The C-terminal residues are highly conserved in most of the species but N-terminal residues are differed. The sequence analysis of HutP results is shown in (Figure S1).

3.2. Structure based analysis

The structure based alignment was done using Dali server [22]. About 716 structures share the similarity with *Z*-score value varying from 2 to 25. A total of 11 structures possess *Z*-score range of 19–25 and belong to HutP family derived with rmsd values 1.4–2.2 Å from *B. subtilis*.

3.3. Structure refinement

The structure of HutP–L-histidine–Mg^{2+} complex was solved by molecular replacement (MR) method using 2ZH0 as template. Structure solution, model building and refinement were carried out through (PHASER, MOLREP, REFMAC) CCP4i suite [23] and Phenix [24]. The model was further improved by using the COOT program [25]. The structure was refined with acceptable stereochemistry and the final *R*-factor is 0.17 (R_{free} 0.23) at 1.9 Å resolution. The Fo–Fc map shows clear density for the metal binding and L-histidine active sites.

The EDTA treated crystal structure of HutP–L-histidine–Mg^{2+} complex is also solved by MR using the above structure as a model

Table 1
Data collection statistics of ternary and EDTA treated ternary complex of HutP from *G. thermodenitrificans*.

Crystal parameters	HutP–L-histidine–Mg^{2+} complex	EDTA treated HutP–L-histidine–Mg^{2+} complex
Data collection		
Space group	$P6_3$	$P6_3$
Unit cell (Å)	a = 90.811; b = 90.811; c = 76.672	a = 91.778; b = 91.778; c = 76.744
No. of molecules in ASU	2	2
Solvent content	56.15	57.84
Resolution range (Å)	50.0–1.91 (outer shell 1.94–1.91)	50.0–2.50 (outer shell 2.54–2.50)
Total reflections	764,204	784,215
Unique reflections	27,990 (outer shell 1388)	12,816 (outer shell 1278)
Redundancy	14.5 (16.0)	11.2 (11.0)
R merge (%)	0.071 (0.449)	0.085 (0.657)
Refinement		
Resolution range (Å)	35.01–1.91	35.31–2.50
R_{work}/R_{free}	0.17/0.23	0.17/0.24
Number protein atoms	2250	2250
Number of ligand atoms	2	2
Number of Mg^{2+} ions	6	2
Number of water molecules	211	72
Rmsd bond lengths (Å)	0.0213	0.0135
Rmsd bond angel (°)	1.9506	1.6060
Ramachandran statistics		
Most favored regions (%)	95.14	95.14
Allowed regions (%)	4.86	4.17
PDB ID	4OK9	4OKQ

R merge = $\sum h \sum i|I(h, i)-\langle I(h)\rangle|/\sum h \sum i\ I(h, i)$, where $I(h, i)$ is the intensity value of the i th measurement of h and $\langle I(h)\rangle$ is the corresponding mean value of $I(h)$ for all i measurements.

template. The Fo–Fc map clearly shows the density for L-histidine and Mg^{2+} ion. The final R-factor is 0.18 (R_{free} 0.23) at 2.5 Å resolution.

3.4. Structure of HutP–L-histidine–Mg^{2+}complex

HutP is a 16 kDa protein crystallized in hexagonal space group ($P6_3$) with two molecules in the asymmetric unit. The homo dimer of each chain consists of 146 amino acids (4–149) (Fig. 2A), one L-histidine ligand, three Mg^{2+} ions and 211 water molecules in total. The first three amino acids are not included in the model due to lack of electron density.

Each monomer of HutP is arranged with four β-strands (β1, β2, β3, β4) and four α-helices (α1, α2, α3, α4). The overall secondary structure possesses a novel folding state wherein the four β-strand sit in the middle of the structure to form an antiparallel β-sheets but α-helices are in the front and back of the β-sheet. The α-helices and β-strands are connected through L1, L2, L3, L4, and L5 loops, a common feature observed in HutP structure of *B. subtilis*. The three dimers of HutP molecules are associated by 3-fold symmetry to form the hexameric structure of HutP (Fig. 2B), which is required for its biological activity. The solvent accessibility surface area (ASA) calculation reveals that the buried surface area by dimer–dimer association and the hexameric HutP has lost the volume of about 3738 Å^2.

4. Discussion

HutP fails to bind with mRNA without L-histidine and the divalent metal ions. The primary amino acid sequence of HutP derived from *G. thermodenitrificans* indicates that the active site residues are highly conserved and similar to *B. subtillis*.

In our complex structure, the high quality difference Fourier map clearly show the electron density map for L-histidine and metal binding sites unambiguously as observed in *B. subtilis*. The bound Mg^{2+} ions have six coordination sphere around with His74, His78, His139, Tyr70 and L-histidine binds with water molecules, hydrogen bonded to OH group of 70Tyr, and with Mg^{2+} ion (Fig. 2C).

In the homo dimer structure, there are four salt bridges which paved the way for the stability and these bridges form the interactions between chains A & B through the amino acids A11Arg-B20Asp, A20Asp-B11Arg, A82Glu-B89Arg, A89Arg-B82Glu (Figure S2).

While modeling both the chains A & B, a couple of additional peaks with appreciable densities in Fo–Fc map were observed around the region of Glu93 and Asp96. This confirms the presence of metal ion (Mg^{2+}) ion and coordinates with Glu93 and Asp96 (Fig. 2C) in contrast to Leu93 and Ser96 in *B. subtilis*. The Mg^{2+} ion is disordered with the symmetry related molecule in both A & B chains. Similar features were observed in the earlier report while crystallizing the *B. subtilis* HutP with high concentration of metal ion, which leads to non-specific metal binding in HutP [14].

When we compare the ternary and EDTA treated ternary complex, the overall shape of both the structures possesses same architecture, whereas the EDTA treated structure lacks density at the non-specific metal binding site. The L3 loop region is altered and slight disturbance is noted due to the removal of Mg^{2+} ions (Fig. 3).

The HutP structure derived from *G. thermodenitrificans* is compared with different complex structures of *B. subtillis*. The structural aspects varies and evident from the increasing values of rmsd, i.e., apo HutP (1WPS) > HutP–HBN complex (1VEA) > HutP–L-histidine–Mg^{2+}–RNA complex (1WMQ).

The ternary complex, the N-terminal α1 helix and the L3 loop regions deviate from the HutP of *B. subtillis* due to the variation in amino acid sequences, non-specific metal binding. L-histidine binding regions α4 (His74, His78, Tyr70) & β4 (His139) involve the structural rearrangements and non-specific metal binding.

Biochemical studies indicate that the termination occurs in *hut* mRNA structure between *hutP* and *hutH* genes within *hut* operon at +498 to +572 [26]. It is known that HutP from *B. subtillis* binds with RNA in the presence of divalent metal ions and L-histidine ligand but fails to bind in the absence of metal ions and ligand [2,26]. Conformational changes are induced in the protein structure during ligand and metal binding which play a vital role in RNA binding of HutP [14]. Once the protein binds with RNA, it regulates the gene expression by destabilizing the terminator structure.

The 21mer RNA **5′-UUUAGUUUUUAGUUUUUAGUU-3′** is used for complex preparation. Each HutP monomer of *B. subtilis* recognizes one UAG motif, particularly at the position of A4 and G5

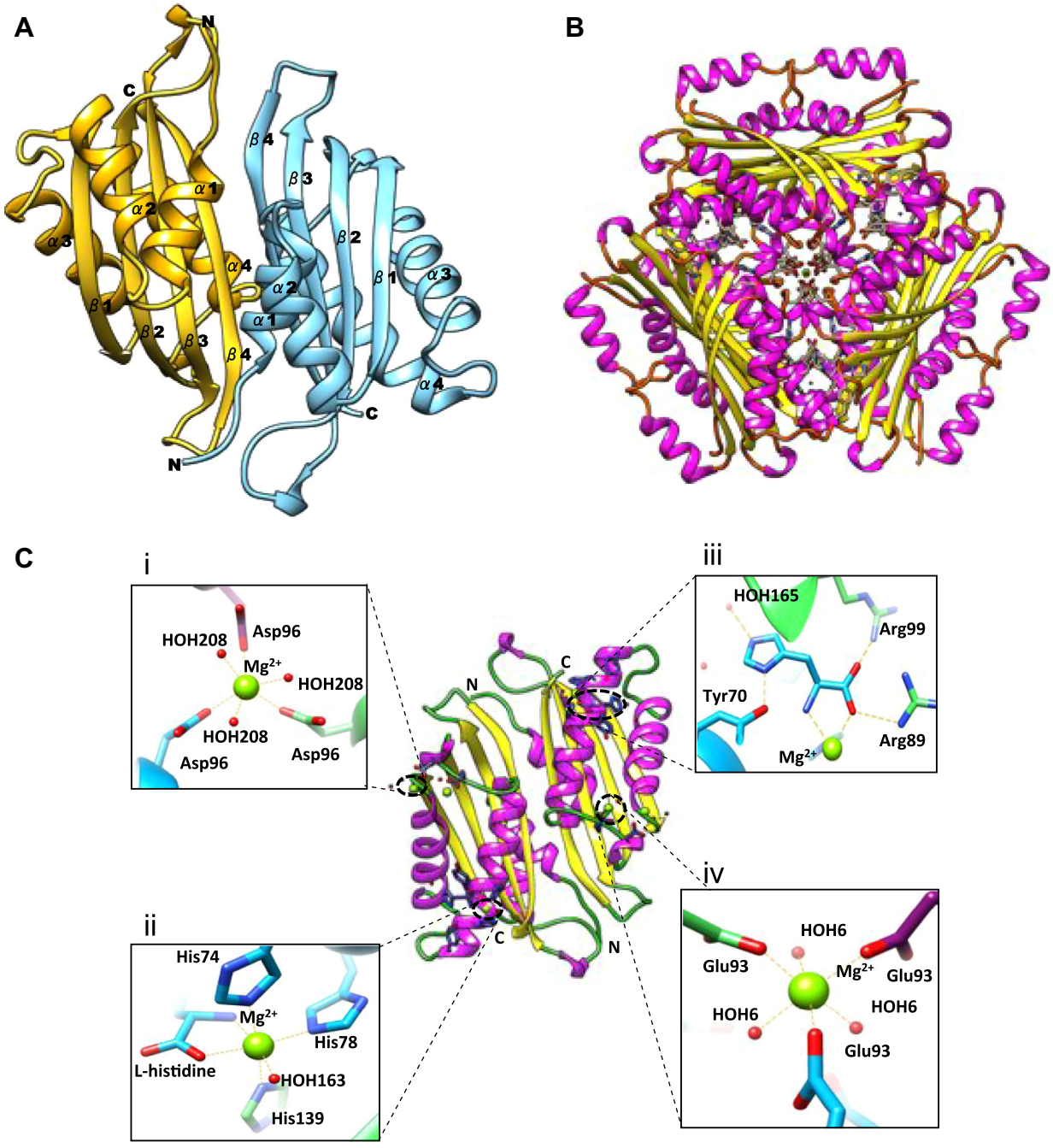

Fig. 2. Crystal structure of *G. thermodenitrificans* HutP ternary complex shown as ribbon representations. (A) Dimeric structure of HutP, (B) hexameric form of HutP, (C) active site, the closer view of ligand and metal binding region (i) the non-specific Mg^{2+} interact with HOH and 96Asp residue, Cyan main chain; Green and Purple are symmetry related molecules, (ii) Mg^{2+} binding with 74His, 78His,139His, L-histidine ligand & HOH molecule, (iii) L-histidine binding with 70Tyr, Mg^{2+}, 99Arg, 89Arg, and HOH molecule,(iv) Second Non specific Mg^{2+} binding with HOH and 93Glu, residue Cyan main chain; Green and Purple symmetry related molecules. Interacting residues are labeled and shows as stick model, Mg^{2+} and water molecules are show as spheres. (For interpretation of the references to color in this figure legend, the reader is referred to the web version of this article.)

bases. The 2′ hydroxyl group of A4 form hydrogen bonds with Thr99, which are the essential interactions in the protein–RNA complexes [27]. In the complex, hydrogen bonding interactions between protein and RNA are contributed by bases and sugars.

Biochemical and crystallographic studies confirm that Glu55, Thr56, Thr99, Thr128 and Glu137 are the key residues for protein–RNA interactions in the complex. Mutagenic analysis indicate that mutated sites at Thr99Ala and Glu137Ala fail to binds with RNA and Thr128Ala reduces the binding affinity up to 15 folds; Glu55 and Thr56 are not involved directly in the interactions, but they provide additional support by acting as spacers during complex formation [13,28].

The conformational changes in HutP from *B. subtilis* during the binding of ligand and metal are already reported [14]. In order to confirm the binding capability of RNA with the HutP from *G. thermodenitrificans*, the crystal structure of HutP–L-histidine–Mg^{2+} is superimposed with HutP–L-histidine–Mg^{2+}–RNA and apo forms of *B. subtilis* (Figure S3). It is inferred (Figure S3) that the

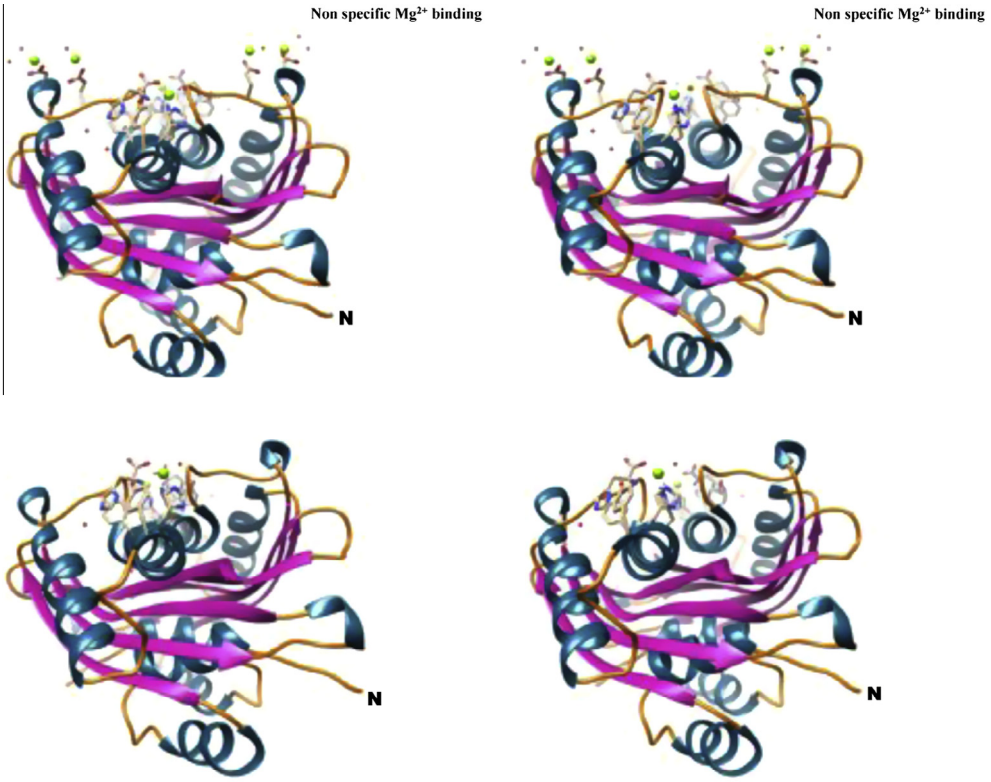

Fig. 3. Stereo view of *G. thermodenitrificans* ternary and EDTA treated ternary complex structures. (A) HutP ternary complex with specific and non-specific metal ions, (B) EDTA treated ternary complex, non-specific metal ions are removed by EDTA chelation. Metal ions are shows in sphere, binding site residues are shown as stick model.

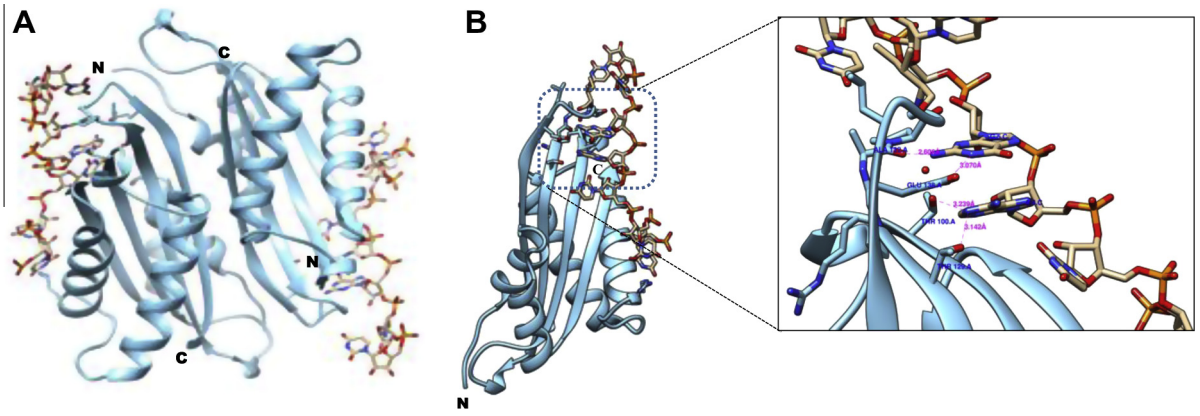

Fig. 4. Proposed HutP–RNA complex structure for G. (A) the quaternary complex structure proposed for Geotn HutP shown in cartoon representation, (B) close-up view of residues involving protein–RNA interactions.

ternary complexes of both proteins are similar and support the binding of RNA with HutP–L-histidine–Mg^{2+} structure of *G. thermodenitrificans*.

The HutP–RNA binding is observed through the gel mobility shift assays using native-PAGE. When the composition of quaternary complex (HutP–RNA–L-histidine–Mg^{2+}) was achieved, the sudden band shift was observed. However, in the absence of any of these parameters (L-histidine/Mg^{2+}) from the above said combination, HutP fails to bind with RNA. This has been experimentally verified by gel shift assay (Fig. 1C). The superposition of ternary complex from *G. thermodenitrificans* with binary and quaternary complex of *B. subtilis* are shown in (Figure S4A). The residual *b*-factor analysis of the apo and quaternary forms of *B. subtilis* and ternary complex of *G. thermodenitrificans* are calculated and shown in (Figure S4B). It is evident that the quaternary complex of *B. subtilis* and ternary structure of *G. thermodenitrificans* show appreciable similarity. This supports to propose protein–RNA complex structure.

Based on gel shift assay, *b*-factor analysis and conformational similarity, a protein–RNA model for *G. thermodenitrificans* has been proposed (Fig. 4). The proposed model resemble with that of the quaternary structure derived from *B. subtilis* which is evidenced from the interactions (Table 2) and the conformation as shown in (Fig. 4A and B). Taken altogether, *G. thermodenitrificans* HutP also regulate the gene expression by an antitermination mechanism identically as explained previously for *B. subtilis*.

In summary, crystal structure of HutP ternary complex (HutP–L-histidine–Mg^{2+}) at high resolution was determined. The gel shift analyses confirm that 21-mer RNA can bind with HutP

Table 2
Protein–RNA interaction residues between *Bacillus subtilis* RNA complex and proposed RNA model of *G. thermodenitrificans*.

Bacillus subtilis RNA complex (1WMQ)	Proposed RNA model for *G. thermodenitrificans*
99 Thr OG1-4A CO2	100 Thr OG1-4A N3
128 Thr OG1-4ACN1	129 Thr OG1-4A CN1
137 Glu OE1-5GCN2	138 Glu OE1-5G CN2
131 Ala-5GCN2	132 Ala-5G CN2
–	133 Pro-5G CO2
–	61 Arg NE-1U CO4

only in the presence of L-histidine and Mg^{2+}. The ternary complex treated with EDTA facilitates the removal of only the non-specific metal ions through chelation. Based on this result, we built the model for the quaternary complex (HutP–L-histidine–Mg^{2+}–RNA) and explain the gene regulatory mechanism and this analysis confirms that HutP protein adopts similar mode of antitermination mechanism between the species. Further biochemical studies will explain the complex dissociation and structural rearrangement upon metal chelation.

Acknowledgments

We thank Ms. M. Okada for the experimental help. We also thank Dr. T. Ishikawa and Ms. Y. Matsumoto for moral support and encouragement. VT and MNP thanks for RIKEN SPring-8 Center for the RIKEN-Internship and Beam line access for data collection.

Appendix A. Supplementary data

Supplementary data associated with this article can be found, in the online version, at http://dx.doi.org/10.1016/j.bbrc.2014.03.036.

References

[1] C. Yanofsky, Attenuation in the control of expression of bacterial operons, Nature 289 (1981) 751–758.
[2] M. Oda, N. Kobayashi, M. Fujita, Y. Miyazaki, Y. Sadaie, Y. Kurusu, S. Nishikawa, Analysis of HutP-dependent transcription antitermination in the *Bacillus subtilis* hut operon: identification of HutP binding sites on hut antiterminator RNA and the involvement of the N-terminus of HutP in binding of HutP to the antiterminator RNA, Mol. Microbiol. 51 (2004) 1155–1168.
[3] B. Rutberg, Antitermination of transcription of catabolic operons, Mol. Microbiol. 23 (1997) 413–421.
[4] P. Babitzke, J. Yealy, D. Campanelli, Interaction of the trp RNA-binding attenuation protein (TRAP) of *Bacillus subtilis* with RNA: effects of the number of GAG repeats, the nucleotides separating adjacent repeats, and RNA secondary structure, J. Bacteriol. 178 (1996) 5159–5163.
[5] J. Otridge, P. Gollnick, MtrB from *Bacillus subtilis* binds specifically to trp leader RNA in a tryptophan-dependent manner, Proc. Natl. Acad. Sci. U S A 90 (1993) 128–132.
[6] P. Babitzke, C. Yanofsky, Reconstitution of *Bacillus subtilis* trp attenuation in vitro with TRAP, the trp RNA-binding attenuation protein, Proc. Natl. Acad. Sci. U S A 90 (1993) 133–137.
[7] A.A. Antson, J. Otridge, A.M. Brzozowski, E.J. Dodson, G.G. Dodson, K.S. Wilson, T.M. Smith, M. Yang, T. Kurecki, P. Gollnick, The structure of trp RNA-binding attenuation protein, Nature 374 (1995) 693–700.
[8] L.A. Chasin, B. Magasanik, Induction and repression of the histidine-degrading enzymes of *Bacillus subtilis*, J. Biol. Chem. 243 (1968) 5165–5178.
[9] Y. Kimhi, B. Magasanik, Genetic basis of histidine degradation in *Bacillus subtilis*, J. Biol. Chem. 245 (1970) 3545–3548.
[10] M. Oda, A. Sugishita, K. Furukawa, Cloning and nucleotide sequences of histidase and regulatory genes in the *Bacillus subtilis* hut operon and positive regulation of the operon, J. Bacteriol. 170 (1988) 3199–3205.
[11] K. Yoshida, H. Sano, S. Seki, M. Oda, M. Fujimura, Y. Fujita, Cloning and sequencing of a 29 kb region of the *Bacillus subtilis* genome containing the hut and wapA loci, Microbiology 141 (Pt 2) (1995) 337–343.
[12] T.S. Kumarevel, Z. Fujimoto, H. Mizuno, P.K. Kumar, Crystallization and preliminary X-ray diffraction studies of the metal-ion-mediated ternary complex of the HutP protein with L-histidine and its cognate RNA, Biochim. Biophys. Acta 1702 (2004) 125–128.
[13] T. Kumarevel, Z. Fujimoto, P. Karthe, M. Oda, H. Mizuno, P.K. Kumar, Crystal structure of activated HutP; an RNA binding protein that regulates transcription of the hut operon in *Bacillus subtilis*, Structure 12 (2004) 1269–1280.
[14] T. Kumarevel, H. Mizuno, P.K. Kumar, Characterization of the metal ion binding site in the anti-terminator protein, HutP, of *Bacillus subtilis*, Nucleic Acids Res. 33 (2005) 5494–5502.
[15] N. Ivanova, A. Sorokin, I. Anderson, N. Galleron, B. Candelon, V. Kapatral, A. Bhattacharyya, G. Reznik, N. Mikhailova, A. Lapidus, L. Chu, M. Mazur, E. Goltsman, N. Larsen, M. D'Souza, T. Walunas, Y. Grechkin, G. Pusch, R. Haselkorn, M. Fonstein, S.D. Ehrlich, R. Overbeek, N. Kyrpides, Genome sequence of *Bacillus cereus* and comparative analysis with *Bacillus anthracis*, Nature 423 (2003) 87–91.
[16] H. Takami, K. Nakasone, Y. Takaki, G. Maeno, R. Sasaki, N. Masui, F. Fuji, C. Hirama, Y. Nakamura, N. Ogasawara, S. Kuhara, K. Horikoshi, Complete genome sequence of the alkaliphilic bacterium *Bacillus halodurans* and genomic sequence comparison with *Bacillus subtilis*, Nucleic Acids Res. 28 (2000) 4317–4331.
[17] H. Takami, Y. Takaki, G.J. Chee, S. Nishi, S. Shimamura, H. Suzuki, S. Matsui, I. Uchiyama, Thermoadaptation trait revealed by the genome sequence of thermophilic *Geobacillus kaustophilus*, Nucleic Acids Res. 32 (2004) 6292–6303.
[18] X.H. Chen, A. Koumoutsi, R. Scholz, A. Eisenreich, K. Schneider, I. Heinemeyer, B. Morgenstern, B. Voss, W.R. Hess, O. Reva, H. Junge, B. Voigt, P.R. Jungblut, J. Vater, R. Sussmuth, H. Liesegang, A. Strittmatter, G. Gottschalk, R. Borriss, Comparative analysis of the complete genome sequence of the plant growth-promoting bacterium *Bacillus amyloliquefaciens* FZB42, Nat. Biotechnol. 25 (2007) 1007–1014.
[19] L. Feng, W. Wang, J. Cheng, Y. Ren, G. Zhao, C. Gao, Y. Tang, X. Liu, W. Han, X. Peng, R. Liu, L. Wang, Genome and proteome of long-chain alkane degrading *Geobacillus thermodenitrificans* NG80-2 isolated from a deep-subsurface oil reservoir, Proc. Natl. Acad. Sci. U S A 104 (2007) 5602–5607.
[20] Y. Tanaka, M. Tawaramoto-Sasanuma, S. Kawaguchi, T. Ohta, K. Yoda, H. Kurumizaka, S. Yokoyama, Expression and purification of recombinant human histones, Methods 33 (2004) 3–11.
[21] S.F. Altschul, W. Gish, W. Miller, E.W. Myers, D.J. Lipman, Basic local alignment search tool, J. Mol. Biol. 215 (1990) 403–410.
[22] L. Holm, S. Kaariainen, P. Rosenstrom, A. Schenkel, Searching protein structure databases with DaliLite v. 3, Bioinformatics 24 (2008) 2780–2781.
[23] N. Collaborative, Computational project, the CCP4 suite: programs for protein crystallography, Acta Crystallogr. D Biol. Crystallogr. 50 (1994) 760–763.
[24] P.D. Adams, P.V. Afonine, G. Bunkoczi, V.B. Chen, I.W. Davis, N. Echols, J.J. Headd, L.W. Hung, G.J. Kapral, R.W. Grosse-Kunstleve, A.J. McCoy, N.W. Moriarty, R. Oeffner, R.J. Read, D.C. Richardson, J.S. Richardson, T.C. Terwilliger, P.H. Zwart, PHENIX: a comprehensive Python-based system for macromolecular structure solution, Acta Crystallogr. D Biol. Crystallogr. 66 (2010) 213–221.
[25] P. Emsley, K. Cowtan, Coot: model-building tools for molecular graphics, Acta Crystallogr. D Biol. Crystallogr. 60 (2004) 2126–2132.
[26] M. Oda, N. Kobayashi, A. Ito, Y. Kurusu, K. Taira, Cis-acting regulatory sequences for antitermination in the transcript of the *Bacillus subtilis* hut operon and histidine-dependent binding of HutP to the transcript containing the regulatory sequences, Mol. Microbiol. 35 (2000) 1244–1254.
[27] T.S. Kumarevel, S.C. Gopinath, S. Nishikawa, H. Mizuno, P.K. Kumar, Identification of important chemical groups of the hut mRNA for HutP interactions that regulate the hut operon in *Bacillus subtilis*, Nucleic Acids Res. 32 (2004) 3904–3912.
[28] T. Kumarevel, H. Mizuno, P.K. Kumar, Structural basis of HutP-mediated anti-termination and roles of the Mg2+ ion and L-histidine ligand, Nature 434 (2005) 183–191.